Reducing the surface roughness beyond the pulsed-laser-deposition limit

E. Vasco,[1] C. Polop,[2] and J. L. Sacedón[1]
[1]*Instituto de Ciencia de Materiales de Madrid, Consejo Superior de Investigaciones Científicas, 28049 Madrid, Spain*
[2]*Depto. Física de la Materia Condensada, Universidad Autónoma de Madrid, 28049 Madrid, Spain*
(Received 22 April 2009; revised manuscript received 8 September 2009; published 23 October 2009)

Here, we outline the theoretical fundamentals of a promising growth kinetics of films from the vapor phase, in which pulsed fluxes are combined with temperature transients to enable short-range surface relaxations (e.g., species rearrangements) and to inhibit long-range relaxations (atomic exchange between species). A group of physical techniques (fully pulsed thermal and/or laser depositions) based on this kinetics is developed that can be used to prepare films with roughnesses even lower than those obtained with pulsed-laser deposition, which is the physical vapor-phase deposition technique that has produced the flattest films reported so far.

DOI: 10.1103/PhysRevE.80.041604 PACS number(s): 81.15.Aa, 68.55.−a, 68.43.Jk

I. INTRODUCTION

In processes between massive systems (e.g., the exchange of atoms between phases by condensation or evaporation), the roughness of the interface between them often has a catalytic effect by creating a network of sites where the rate of the processes is higher. Some examples of processes catalyzed by interface roughness are (i) abrupt phase changes [1] such as boiling and precipitation, (ii) reactions with propagation fronts in a disordered medium [2] (e.g., wetting, cracking, and combustion), and (iii) transport-limited surface reactions [3] (oxidation and impurity adsorption). Some of these processes have a pernicious influence on commonly used procedures in microelectronics and nanotechnology. Thus, for example, intrinsically inert surfaces of different natures [such as Ag(001) and graphite(0001) at temperatures as low as 105 K] oxidize when their roughnesses increase as demonstrated [4] in experiments of roughness induced by ion bombardment. Whereas nanostructuring methods for the preparation of macroscopic arrays of size-, shape- and symmetry-tailored nanostructures have been well established [5], methods for flattening [6] crystalline interfaces are yet to be developed.

Pulsed laser deposition (PLD) is a physical vapor-phase deposition (PVD) technique that recent studies [7–9] have demonstrated suitable for the preparation of ultraflat ultrathin films with intrinsic [10] roughnesses lower than those obtained with other techniques such as molecular beam epitaxy (MBE), sputtering, pulsed thermal deposition [11] (PTD), and growth methods assisted by ion beams [12] and/or energetic particles in the deposition flux [13,14] This advantage is due to the distinctive coarsening mechanism (identified [9] as kinetically limited Ostwald ripening) of growth in PLD, which results from (i) the supersaturation of the pulsed flux that gives rise to a nonequilibrium density [15,16] of small surface species immersed in a monomer-depleted background, and (ii) the hyperthermal nature of the incident atoms, which shifts the size distribution of the species population up to larger sizes. The combination of the two effects [(i) and (ii)] gives rise to a high density of moderate-sized clusters (tetramers to septamers) [16], which are small enough to prevent top-layer nucleation and large enough to be kinetically stable. Thus, the PLD technique promotes layer-by-layer growth. In contrast, continuous flux-based techniques produce a surface-species distribution consisting mostly of islands (octamers and larger) [9,16] that coarsen quickly from the monomer background. This background is fed continuously by the flux and/or cluster breakup in growths assisted with energetic particles [12,13]. The resulting islands are large enough to allow top-layer nucleation and so result in multilayer growth and an inherently greater roughness.

In this work, we design an optimal growth kinetics, which we call *fully pulsed growth kinetics*, which can be used in the preparation of the flattest films—even flatter than those grown with PLD. To realize this kinetics experimentally, we propose modifications of the PLD and PTD techniques in which steady growth temperatures are replaced with temperature transients induced by a chopped infrared laser [17] focused on the surface of growing films. These modified techniques are denoted here full-PLD (FPLD) and full-PTD (FPTD).

II. MODELING

The model we used to characterize the growth kinetics (and thus the resulting morphology) of the investigated PVD techniques (namely, PTD and PLD and their fully pulsed counterparts FPTD and FPLD, respectively) is summarized in their generalized forms,

$$\frac{\partial \rho_n^k}{\partial t} = M^{k-1}\rho_m^{k-1}\tilde{F}(t)[A_{n-1}\rho_{n-1}^k - A_n\rho_n^k] + \sum_{i=1}^{n-1}(1+\delta_{i,n-i})D_i\sigma_{n-i}\rho_i^k\rho_{n-i}^k + -\sum_{i=1}^{n_c,m}(D_i\sigma_n + D_n\sigma_i)\rho_i^k\rho_n^k + \frac{1}{2}\sum_{i=n+1}^{n_c}(\Gamma_i^n + \Gamma_i^{i-n})\rho_i^k - \frac{1}{2}\sum_{i=1}^{n-1}(1+\delta_{i,n-i})\Gamma_n^i\rho_n^k - \varepsilon_n\delta_{n,1}\rho_n^k - D_n\delta_{k,1}\nabla^2\rho_n^k, \quad (1a)$$

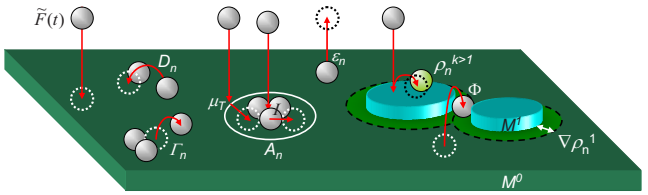

FIG. 1. (Color online) Schematic representation of the processes considered in our model [Eqs. (1a)–(1c)]. The sketched species correspond to mobile species (ball model), islands (solid disks), and substrate (slab M^0). The represented processes are (from left to right) time-dependent flux ($\tilde{F}$), nucleation and aggregation by diffusion of mobile species (D_n), dissociation of species (Γ_n), species coarsening via direct incidence with atomic insertion (I) or indirect incidence with capture in the surrounding area A_n by transient mobility (μ_T), re-evaporation of species (ε_n), island coalescence (Φ), depletion of monomers around the islands ($\nabla\rho_n^1$) where the depleted areas are encircled, and top-layer nucleation and aggregation ($\rho_n^{k>1}$).

$$\frac{\partial \rho_m^k}{\partial t} = M^{k-1}\rho_m^{k-1}\tilde{F}(t)[A_{n_c}\rho_{n_c}^k] + \sum_{i=1}^{n_c}(1+\delta_{i,n_c+1-i})D_i\sigma_{n_c+1-i}\rho_i^k\rho_{n_c+1-i}^k - \rho_m^k\left(\rho_m^k\sqrt{M^k}\sum_{i=1}^{n_c} iD_i\rho_i^k\right), \tag{1b}$$

$$\frac{\partial M^k}{\partial t} \approx \sqrt{M^k}\sum_{i=1}^{n_c} iD_i\rho_i^k + M^k\left(\rho_m^k\sqrt{M^k}\sum_{i=1}^{n_c} iD_i\rho_i^k\right), \tag{1c}$$

which were succinctly described elsewhere [9,16]. The atomic processes considered in the model are sketched in Fig. 1. The model is based on a partial differential equation system (PDES) of rate equations, which describes the time evolution per k-indexed monolayer (ML) deposited successively on a substrate (with $k=0$) of [Eqs. (1a) and (1b)] the densities of surface species, where ρ_n^k [Eq. (1a)] is the density of n-sized mobile species from monomers up to n_c-sized species ($n=1,\ldots,n_c$) and ρ_m^k [Eq. (1b)] is the density of islands (immobile stable species with sizes $>n_c$) added together by means of a generic index m; and [Eq. (1c)] the average size in number of atoms of the islands (M^k). The PDES [Eqs. (1a)–(1c)] is strongly coupled for species of different sizes adsorbed in the same ML (those with the same index k) and weakly coupled between MLs (with different k up to 6 ML). n_c denotes the critical size that determinates the crossover between two-dimensional (2D) and three-dimensional (3D) growth modes of the surface species as discussed below. The model considers the mobility of all species with sizes $n \leq n_c$ and assumes them a limitless capacity for the morphological relaxation toward 2D compact shapes via interlayer transport. On the contrary, the weak coupling between MLs is performed by considering tops of the islands (with sizes $>n_c$) to be the confinement regions for the mobile species, which is equivalent to suppose a strong step-edge barrier at the island border that inhibits the interlayer transport and enables the top-layer nucleation. The model assumes that the growth occurs in homoepitaxy conditions on a massive singular substrate ($M^0\rho_m^0=1$) to avoid any influence of the substrate structure on the morphological evolution of the surfaces simulated for the investigated growth kinetics. The model comprises the following processes (sketch in Fig. 1).

First term in Eqs. (1a) and (1b) accounts for the formation or decay of species due to the random incidence $\tilde{F}(t)$ of thermal monomers (for PTD and FPTD, with kinetic energy $E^{kin}<1$ eV—details in Ref. [18]) or hyperthermal ones (for PLD and FPLD, with [18] $E^{kin}\sim 1-24$ eV). The random incidence is simulated to occur in the form of $t_F=1$ ms flux pulses, separated from each other by $1/\nu_F=1$ s, at a deposition rate of $F=0.1$ ML/s. Time-dependent $\tilde{F}(t)$ is defined then as $\tilde{F}(t)=(F/\nu_F t_F)U[t_F-t']$, where $U(x)$ is the unit-step function and t' is the time lapsed from the beginning of the previous pulse computed as the remainder of the division $t/(1/\nu_F)$. $A_n \approx (\sqrt{n}+R/\sqrt{n})^2$ denotes the capture area of incident atoms by n-sized species ($n \leq n_c$) considering transient mobility [19] (mechanism labeled μ_T in Fig. 1) and atomic insertion (mechanism labeled I). The contribution of the transient mobility to A_n is described in terms of the capture radius R for monomers deposited beyond the species edge. Thus, R depends on E^{kin} of the incident monomers as follows: (i) for thermal monomers captured by direct incidence, $R=0 \Rightarrow A_n=n$, whereas (ii) for hyperthermal ones captured by transient mobility, $R=0.54$ unit-cell lattice (see Ref. [19]) ≈ 1 site from the species edge $\Rightarrow A_n > n$. The division $R/\sqrt{n}$ in the expression of A_n takes into consideration that the perimeter sites of an n-sized species ($\propto\sqrt{n}$) share free nearest-neighboring sites. The factor $(M^{k-1}\rho_m^{k-1})$ in Eqs. (1a) and (1b) accounts for the top-layer nucleation of the kth ML on the islands belonging to the $(k-1)$th ML.

Second and third terms in Eq. (1a) and second one in Eq. (1b) correspond to the formation or decay due to the aggregation by random walk diffusion of the mobile species in nonconfined (substrate surface, $M^0 \to \infty$) and confined regions (tops of the islands of finite size M^k). The diffusion occurs at a region-size-dependent rate $D_n \equiv D_n(M^k) = [D_n(M^k \to \infty)]^2/\min[D_n(M^k \to \infty), M^k\sqrt[3]{\ln(M^k)}]$, in which $D_n=[D_n(M^k \to \infty)]^2/M^k\sqrt[3]{\ln(M^k)}$ (diffusion coefficient for confined regions) considers the logarithmic correction for Brownian motions. This correction takes into account that the probability of visiting the surface sites more than once by random walk increases as the size of the confinement region decreases. Thus, to visit all atop sites of an M^k-sized island [with $M^k \ll$ diffusion length$^2 \propto D_n(M^k \to \infty)$], $M^k\sqrt[3]{\ln(M^k)}$ hops are required [20]. The diffusion is biased by the propensity to capture the involved species given in terms of their coverage-independent capture numbers $\sigma_n \propto \sqrt{n}$. The factor $1+\delta_{i,n-i}$ (where $\delta_{x,y}$ is the Kronecker delta) considers the aggregation to each other of two indistinguishable species with the same size.

Fourth and fifth terms in Eq. (1a) describe the binary dissociation of species (with sizes $n \leq n_c$) at a rate Γ_n^i into a pair of resulting species of sizes i and $n-i$. $\frac{1}{2}\Sigma$ in the fourth and fifth terms takes into account that $\Gamma_n^i \equiv \Gamma_n^{n-i}$ are referred to the same process.

Sixth term in Eq. (1a) denotes the re-evaporation of species at a rate ε_n. Our model considers only the monomer

re-evaporation ($\varepsilon_n \delta_{n,1}$) on the basis of assuming plausibly [16] the dissociation of the species into monomers and their later re-evaporation as energetically more favorable than the re-evaporation of species as a whole.

First term in Eq. (1c) describes the coarsening of the islands that occurs at a rate $\sqrt{M^k}\Sigma_{i=1}^{n_c} iD_i\rho_i^k$ via the capture of mobile species.

Third term in Eq. (1b) and second one in Eq. (1c) describe the effect of the island coalescence on the island density ρ_m^k and the island coarsening $\partial M^k/\partial t$, respectively. The model assumes the coalescence of compact-shaped islands (mechanism Φ in Fig. 1), such that the characteristic time of coalescence is defined as that required for an island that grows via the capture of mobile species at a rate $\sqrt{M^k}\Sigma_{i=1}^{n_c} iD_i\rho_i^k$ [see first term in Eq. (1c)] to fill the surrounding area $1/\rho_m^k$ that is free of other islands.

Last term in Eq. (1a) takes into consideration the depletion of mobile species (mostly monomers) close to the islands through a lattice-depletion approximation [21]. The depleted regions (denoted $\nabla\rho_n^1$) are depicted in Fig. 1. The model assumes that these regions are distributed around the positions of the islands, which are arrayed in an $1/\sqrt{\rho_m^1(t)}$-spaced hexagonal lattice. This term accounts for the effective dependence of the capture numbers on coverage, which was not considered in the second and third terms in Eq. (1a) for nonsteady surfaces (e.g., those generated by pulsed growth kinetics) where solutions of the diffusion equation based on Bessel functions are not available [21]. Note that under PLD-type growth kinetics (namely, deposition with highly supersaturated flux pulses on a shorter time scale than that corresponding to the motion of the monomers) neither extra adatom depletion nor large statistical deviation of the species populations (as those predicted for continuous growths in confined geometries) [22] on tops of the islands is expected with regard to the species densities between islands [23,24]. Consequently, the model assumes common rules for both top-layer and substrate-surface nucleation.

The mechanisms included in the first term in Eq. (1a) correspond to nonequilibrium processes that happen during the arrival time of the flux pulse, whereas those considered in the other terms and/or equations describe thermal processes whose occurrence probabilities follow a Poisson distribution. It should be stressed that the proposed model [9,16] was able to get insights into the origin of the exceptionally lower roughness achieved in ultrathin films grown by PLD [7,8], and the simulated results (in particular, the roughness evolution) were in agreement with the experimental data [25] reported for PLD-grown Y-stabilized ZrO_2 (YSZ) films on InP(100).

In a new feature, the model used in this work has been modified to include the time dependence of the growth temperature $T(t)$ (previously treated as steady in Refs. [9,16]), which affects the rates of all the thermally activated processes considered (namely, D_n, Γ_n, and ε_n). The surface temperature $T(t)$ of the growing film (hereafter, temperature transient or T transient) was estimated by means of the heat equation for a $d=1$-mm-thick YSZ bulk on a metal support held in vacuum at a base temperature of $T_0=753$ K. $T(t)$ is generated by the pulsing (pulse width of $t_{IR}=30-300$ ms) of a chopped 100 W-CO_2 laser, which is focused on a spot with size $\vec{r}_{IR}^2$ on the YSZ surface. The calculation of $T(t)$ takes into consideration the heat transfer toward the metal support that results from thermal conduction and neglects losses by radiation due to the relatively low growth temperatures used for the simulations [26]. The equation describing the film surface heating $\rho C_p \partial_t T'(\vec{r},z,t) = -\vec{\nabla}(\kappa\vec{\nabla}T') + \kappa(r_{IR}^2/d)(T_0 - T') + I_{IR}$ for $d \ll r_{IR}$ was numerically solved using semispherical coordinates in 2D+1 dimensions (with $-z$ along the out-of-the-film plane direction) by assuming thermally independent parameters for YSZ [27]. The space and time spread of the laser power within the YSZ bulk is described by $I_{IR}(\vec{r},z,t) = \alpha I_0 U(r_{IR}-r)U(t_{IR}-t)e^{-\alpha z}$ [where $U(x)$ is the unit-step function]. The temperature transient $T(t)$ is then computed as the surface temperature averaged over the laser spot: $T(t) = r_{IR}^{-2} \times \int_{\vec{r}_{IR}} T'(\vec{r}, z \to 0, t)\partial^2\vec{r}$. A time width Δt and a modulation amplitude of the surface temperature $\Delta T = T(t_{IR}) - T_0$ can be ascribed to a given transient $T(t)$ from the condition $t_{IR}\Delta T = \int_0^{\Delta t}[T(t)-T_0]\partial t$, which defines an equivalent square-pulsed transient. Temperature transients with various widths ($\Delta t = 50$, 100, 250, and 500 ms) and similar amplitudes [$\Delta T \approx 120$ K from $T_0=753$ K up to $T(t_{IR}) \approx 873$ K] were computed from the laser parameters in Ref. [28] and used to simulate the fully pulsed growth kinetics.

The model (described through a PDES of $\max(k) \times (n_c + 2)$ equations: $\partial\rho_1^k/\partial t \ldots \partial\rho_{n_c}^k/\partial t$ [outlined in Eq. (1a)], $\partial\rho_m^k/\partial t$ [Eq. (1b)], and $\partial M^k/\partial t$ [Eq. (1c)], with $k=1,\ldots,6$ ML) was solved numerically using the standard *method of lines* to discretize the 2D space and then time integrated by the *Runge-Kutta method*. The atomistic nature of the model restricts the simulation scenario to early growth stages since $2\sqrt{2d}+1$ ML is required to address the random deposition of d MLs (in our case, we considered up to $\max(k)=6$ ML for a 3-ML-thick film). Thus the PDES that results of simulating the growth of thicker films would prove numerically intractable. The integration tolerance was chosen to fix the error in the species densities to be lower than 10^{-6} species/site ($\approx \pm 1$ species/200×200 nm^2) during the whole range of simulated thicknesses (0–3 ML). The initial and the lattice-depletion [21] boundary conditions were $\rho_n^k(\vec{r}, t=0)=0$ and $\rho_n^1(\vec{r} \to \vec{r}_m, t) \to 0$, respectively, where $\vec{r}_m$ indicates the positions on the substrate surface of $1/\sqrt{\rho_m^1(t)}$-spaced islands (hexagonally arrayed) that act as sink for mobile species. To compute Eqs. (1a)–(1c), the thermodynamic parameters for species of any size were estimated by applying empirical size-scaling relationships [16,29] to reported values for monomers, which were taken within the representative range for highly corrugated (100) surfaces of perovskite oxides [30] [typically $YBa_2Cu_3O_{7-\delta}$ (Ref. [31]) and $SrTiO_3$ (Ref. [32])]. Once computed, $\rho_n^k(\vec{r},t)$ was averaged over the surface and its evolution together with that of $M^k(t)$ are the mean-field features used to describe the growth kinetics of the studied PVD techniques. The resulting surfaces were investigated with regard to the following: (i) the surface roughness $\omega(t) \approx \sqrt{\Sigma_{k=0}^{\eta}\{\theta^k - \theta^{k+1}\}[k - \int_0^t \tilde{F}(t)\,\partial t]^2}$, where $\theta^k = \Sigma_{i=1}^{n_c} i\rho_i^k + M^k\rho_m^k$ denotes the fractional coverage of kth ML and $\int_0^t \tilde{F}(t)\,\partial t$ corresponds to the film thickness for a minor re-evaporation; (ii) the number of uncovered layers η

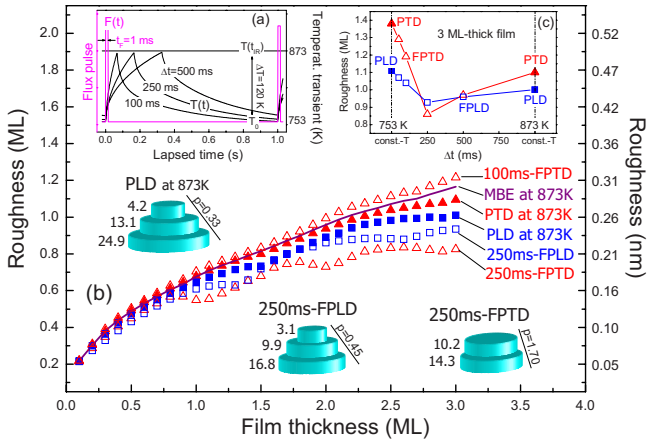

FIG. 2. (Color online) (a) Pulsed flux [curve $F(t)$—with pulse width of $t_F=1$ ms, frequency $\nu_F=1$ Hz, and intensity $F/t_F\nu_F$ plotted in arb. unit] and T transients [curves $T(t)$—with several pulse widths Δt and amplitudes of $\Delta T=120$ K over a common base temperature of $T_0=753$ K, so $\Delta T+T_0=873$ K] used in the simulations of the pulsed growth kinetics. The T transients are generated with a chopped CO_2 laser focused on YSZ surface [25,27,28]. (b) Thickness dependence of the roughness generated at constant $T=873$ K with the PVD techniques: MBE (solid line), PTD (▲), PLD (■), and their fully pulsed counterparts: Δt-FPTD (△) and Δt-FPLD (□) whose time-dependent growth temperatures correspond to the T transients shown in (a). Sketches depict the representative morphologies of surface structures formed at $t=20$ s with PLD, FPTD, and FPLD (for $\Delta t=250$ ms). The numbers correspond to cross sections per ML and p denotes the slope at the structure border. (c) Time-width Δt dependence of the roughness for a 3.0-ML-thick (≈0.8 nm) YSZ film grown by FPTD (△) or FPLD (□). Note that for $\Delta t=0$ s ($\Delta t=1/\nu_F=1$ s), FPTD and FPLD produce similar results to those of PTD (▲) and PLD (■) at constant $T=753$ K (const. $T=873$ K), respectively.

that forms the surface (estimated from the condition $1-[\Sigma_{k=1}^{\eta}\,\theta^k/\int_0^t \tilde{F}(t)\,\partial t]\leq 10^{-2}$ that defines an onset of 0.01 ML of coverage to consider the nucleation of a new ML); and (iii) the representative morphology of the surface structures modeled as a stack of η mean species, each one with the average size per ML considering both mobile species and islands: $\bar{m}^k=\theta^k/[\Sigma_{i=1}^{n_c}\,\rho_i^k+\rho_m^k]$. To overcome the limitations that the model presents to address the ML-completion regime—that occurs through filling the narrow spaces between compact islands with strong step-edge barriers (Zeno effect [33])—a ML-completion onset $\theta_c=0.9$ ML was assumed to recalculate the roughness evolution.

III. RESULTS

A. Result analysis

Figure 2(a) shows the time profiles of the pulsed flux $\tilde{F}(t)$ and temperature transients $T(t)$ used to simulate both semi-pulsed [with $\tilde{F}=\tilde{F}(t)$ and $T=$const; typical of PTD and PLD] and fully pulsed [with $\tilde{F}=\tilde{F}(t)$ and $T=T(t)$; FPTD and FPLD] growth kinetics. The thickness dependences of the surface roughness (ω) in the early stages of growth with the investigated PVD techniques are plotted in Fig. 2(b) together with representative morphologies of the surface structures formed by PLD, FPLD, and FPTD at $t=20$ s. The oscillatory behavior of the roughness evolution (as shown in FPTD, FPLD, and PLD curves) is the result of the ML-completion condition $\theta^k>\theta_c$ assumed above. The no recovery of the roughness toward the initial flat surface values indicates that the completion process of successive MLs is not perfect as the true layer-by-layer growth does not exist (see discussion concerning growth kinetics interpretation by surface diffraction techniques in Ref. [24]) and the generated defects accumulate from layer to layer. As mentioned above [8,9], the surfaces obtained for constant T with techniques based on pulsed fluxes (PTD and PLD) are flatter than those prepared using continuous fluxes (represented here by MBE). The additional use of T transients between $T_0=753$ K and $T(t_{IR})=873$ K (combined with pulsed fluxes in FPTD and FPLD) gives rise to the changes in film roughness shown in Fig. 2(c) as follows: (i) T transients with time widths $\Delta t\geq 250$ ms produce a decrease in the roughness with respect to those achieved with PTD and PLD at constant $T=873$ K; (ii) T transients shorter than 250 ms generate increases in the roughness that tend toward the values obtained with PTD and PLD at constant $T=753$ K. The decrease in the roughness that results of using the T transients is greater in FPTD-grown films ($\omega_{250\ \mathrm{ms\ FPTD}}/\omega_{\mathrm{PTD}}-1\approx -25\%$ for 3-ML-thick films) than in those prepared with FPLD (≈−10%). The minimum value obtained with FPTD is ≈20% lower than the roughness of films grown with PLD, which is the established PVD technique producing the flattest crystalline films so far [7–9]. It should be highlighted that a decrease of 20% (with an extrapolated saturation $\omega<1$ ML) represents a major advance due to the intrinsically discrete nature of the matter at these space scales (namely, ≤3 ML) [34]. The analysis of the representative morphologies of the surface structures shown in Fig. 2(b) reveals that in comparison with PLD, fully pulsed growth kinetics (FPTD and FPLD) generates smaller structures with higher border slopes p. This effect is particularly important for FPTD-grown structures.

B. Explanation of results

To understand the variation of the roughness that results from the use of T transients and, in particular, the origin of the lower roughness achieved with fully pulsed growth kinetics, we need to investigate the balance between competing processes of morphological relaxation and species coarsening. Three relevant processes were considered, which are implicitly or explicitly included in our model. They are (a) the incidence of atoms on top of a 2D n-sized compact species, (b) the escape of atoms from the atop sites of such a species downward free sites at the species border (without detachment) via atomic insertion next to the edge of the species and/or descent across kinks [35], and (c) the atomic exchange between neighboring species via detachment—diffusion—attachment of monomers. In this latter process, we do not distinguish between monomers supplied by the flux (typical of growths with continuous fluxes where the single monomers can be considered as surface species and

thus the detachment is not required) and those generated by species ripening (Ostwald ripening typical of growths with pulsed fluxes [9] where the surface is depleted in monomers and these are generated via detachment from larger species). The characteristic times of the considered processes (namely, t_i^{pul}, the time lapse between successive incidences of atoms coming from a pulsed flux; t_r, the relaxation time between on-top incidence and escape downward; and t_e, the time lapse between successive captures of diffusing monomers) were estimated by means of a mean-field approach as

$$t_i^{pul}(n) = \nu_F^{-1} Q[t_i^{cont}(n)/t_F] + \mathrm{mod}[t_i^{cont}(n)/t_F], \tag{2a}$$

$$t_r(n) = 1/\Phi(n) D_1(n), \tag{2b}$$

$$t_e(n) = \nu_F / F \sigma_n D_1(\infty), \tag{2c}$$

where $t_i^{cont}(n) = \nu_F t_F / nF$ [in Eq. (2a)] is the time lapsed between successive incidences of atoms within a continuous flux with equivalent intensity $F/\nu_F t_F$, $Q(t_i^{cont}/t_F)$ [$\mathrm{mod}(t_i^{cont}/t_F)$] is the integer quotient (remainder) of the division t_i^{cont}/t_F, [Eq. (2b)] $\Phi(n) = \sqrt{n-\Delta}/n-\Delta$ for $n>2$ and $\Phi(n) \approx 1$ otherwise (with $\Delta=2$) is the ratio of edge-atop sites to total-atop sites for an n-sized species that describes the geometric probability of escaping downward (Ref. [36]), and as defined above [second and third terms in Eq. (1a)], $D_1(\infty) \equiv D_1(M^0 \to \infty)$ and $D_1(n)$ are the diffusion coefficients for monomers on the substrate surface [Eq. (2c)] and on tops of the n-sized species [Eq. (2b)], respectively. The physical meanings of Eqs. (2a)–(2c) are described as follows: Eq. (2a) accounts for the pulsed nature of the flux defining the deposition effective time on an n-sized species $t_i^{cont}(n)$ in t_F (pulse-width) units separated to each other by $1/\nu_F$ seconds. t_r is estimated in Eq. (2b) as the time that results from multiplying the number of hops required to escape from top of an n-sized species [$\propto 1/\Phi(n)$] without considering step-edge barrier [35] by the time that takes each hop $1/D_1(n)$. On the other hand, to estimate t_e like the shortest time for the atomic exchange between surface species, Eq. (2c) considers a nonconfined surface that is not fully depleted in monomers so that $t_e \geq t_c$ (where t_c is the time required to capture free monomers without involving detachment). The spacing of the species (some of them monomers) adsorbed on such a surface is [37] $\lambda \sim \sqrt{\nu_F/F}$ (where F/ν_F is the deposition rate per pulse) and consequently using the Einstein relation $t_c \sim \lambda^2/D_1$ can be taken as the lowest limit of t_e.

The dependences of the characteristic times [Eqs. (2a)–(2c)] on the size of the involved species for the specified growth temperatures are shown in Fig. 3(a). The ratio $t_r(n)/t_i^{pul}(n)$ determines the growth mode as follows: (i) if for a given temperature and a certain n-sized species $t_r(n) < t_i^{pul}(n)$ (i.e., the adatom on top of such a species descends before a new atom arrives) the species grows in 2D form; otherwise, (ii) the probability of top-layer nucleation becomes high, and a multilayer 3D growth is promoted. The crossover between 2D and 3D growth modes of the species, which appears due to the increase (decrease) in $t_r(n)$ [$t_i^{pul}(n)$] as the species coarsens (i.e., its size n increases) defines a T-dependent critical size $n_c \equiv n_c^{2D\to 3D}$ that satisfies the condition $t_r(n_c) = t_i^{pul}(n_c)$. Species larger than $n > n_c(T)$ (supercritical ones) for a given temperature T are mostly 3D, and their contribution to the roughness is higher than that of the species with similar sizes and 2D shapes generated at higher temperatures $T+\Delta T$ at which $n_c(T+\Delta T) \geq n$. Thus, for example, as shown in Fig. 3(a) (species represented by a ball model), septamers obtained at $T+\Delta T = 873$ K [where at $t_r(n=7) = 0.19$ s, $t_i^{pul}(7) \approx 1$ s and $n_c = 10$] are 2D, whereas those grown at lower temperatures, e.g., $T = 813$ K [at $t_r(7) = 1.35$ s, $t_i^{pul}(7) \approx 1$ s and $n_c = 5$] are 3D. This explains the increase in the roughness as the growth temperature drops [compare in Fig. 2(c) the roughnesses obtained by PLD and PTD for constant $T = 873$ K with those for constant $T = 753$ K] as a consequence of the decrease in $n_c(T)$ [from

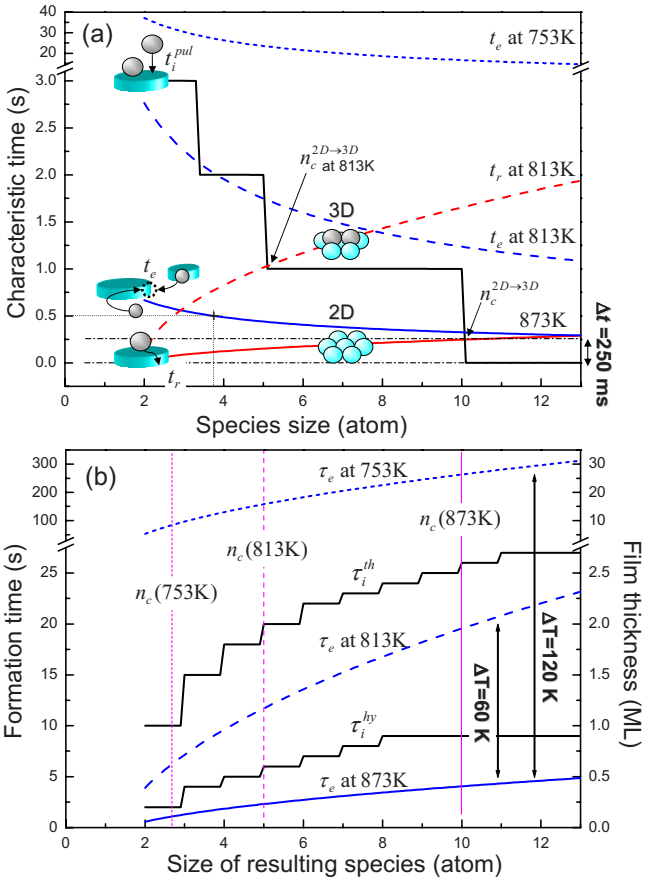

FIG. 3. (Color online) (a) Dependences of the characteristic times of on-top incidence (t_i^{pul}), escape downward (t_r), and atomic exchange (t_e) on the size of the involved largest species for various growth temperatures. The 2D and 3D morphologies of septamers generated at 873 and 813 K, respectively, are sketched by means of a ball model and the corresponding critical sizes $n_c^{2D\to 3D}$ are pointed out. The optimal time width $\Delta t = 250$ ms of the T transient (that satisfies the condition $t_r < \Delta t < t_e$ for $n \leq n_c^{2D\to 3D}$) is indicated on the right margin. (b) Times of formation (and corresponding deposited thickness $F\tau_x$—right-hand axis) of n-sized species via the successive incidence of thermal (τ_i^{th}) and hyperthermal (τ_i^{hy}) atoms or via the atomic exchange (τ_e). The vertical lines denote the values of the temperature-dependent $n_c^{2D\to 3D} = n_c(T)$. The optimal modulation amplitudes $\Delta T = 120$ K and $\Delta T = 60$ K of the T transients for growths with thermal and hyperthermal pulsed fluxes, respectively, are indicated.

$n_c(873\ \mathrm{K})=10$ down to $n_c(753\ \mathrm{K})=3$—value not indicated in Fig. 3(a)]. Thus, to achieve low roughnesses, large values of n_c are required so that it is feasible to generate a high density of subcritical species (those with sizes $n \leq n_c$). Consequently, the proposed model [Eqs. (1a)–(1c)] uses the thus-defined critical size n_c to classify the surface species into species (those with sizes $n \leq n_c$ that possess a limitless capacity for the morphological relaxation toward 2D shapes) and islands (with sizes $>n_c$ and a limited relaxation capacity). This classification allows us to simulate successive growth of MLs (from the bottom layers up to the top ones) by decoupling of the pulsed deposition and the interlayer transport. The decoupling was carried out assuming the interlayer transport by escaping downward from atop sites of the species ($n \leq n_c$) as an instantaneous process whereas the escape from tops of the islands ($n > n_c$) was considered as an inhibited process at the growth time scale, in short, each incident atom arrives on the appropriate ML. This assumption would overestimate the top-layer nucleation rate—considered to be $\approx 1/t_i^{pul}(n)$—on tops of islands free of effective step-edge barriers.

Similarly, the T-dependent ratio $t_e(n)/t_i^{pul}(n)$ determines two regimes of coarsening: (i) for $t_e(n) > t_i^{pul}(n)$, the species grow in an isolated manner only via the incidence of the atoms coming from the pulsed flux (it produces a slow coarsening); (ii) for $t_e(n) < t_i^{pul}(n)$, the species grow mainly by atomic exchange with neighboring species via diffusing monomers (fast coarsening). In the above example [ball model-sketched species in Fig. 3(a)], the 2D septamers grown at 873 K become octamers (i.e., gain an atom) after $t_e(7)=0.4$ s via atomic exchange. This growth of septamers into octamers can be delayed as long as $t_i^{pul}(7)=1.0$ s—for species that coarsen through atomic incidence—by using lower growth temperatures [e.g., $T \leq 813$ K that produce $t_e(7) \geq 1.4$ s]. The recipe for achieving low roughness in this latter case consists of hindering the coarsening (i.e., slowing it as much as possible) to prevent that species reach the critical size n_c quickly and thus to extend the 2D growth mode up to larger thicknesses. In surfaces fully depleted in monomers (for example, in vicinal surfaces [32] due to the preferential capture by the steps) the slow-coarsening condition $t_e(n) > t_i^{pul}(n)$ is permanently fulfilled for the species but not for the terraces (that can be considered as massive species). This produces 2D growth of the species and 3D with top-layer nucleation of the terraces—that are typical modes of growth by step flow [32] in which the deposited material reproduces the 3D vicinal morphology of the substrate. The fact that the relaxation by escaping from atop sites of a species ($n \leq n_c$) is the faster considered process [note in Fig. 3(a) that $t_r(n) \leq t_i^{pul}(n)$ and $t_r(n) < t_e(n)$ for any $n \leq n_c$ at constant T] supports our assumption of decoupling the pulsed deposition and the interlayer transport (see discussion above) due to the reduced capacity of the species to become island before the atoms adsorbed on them can escape downward.

In this context, $t_r(n)$ and $t_e(n)$ can be identified with the characteristic times for short-range (intraspecies) and long-range (interspecies) relaxations, respectively. The use of a temperature transient with time width Δt produces a progressive "freezing" as T decreases of any thermal process with a characteristic time $t > \Delta t$. This means that the processes faster than Δt have a high occurrence probability, whereas the slower ones are partially inhibited on the incidence time scale $t_i^{pul}(n)$ [38], which is temperature-independent. To show the influence on the growth kinetics of a T transient with, for example, $\Delta T + T_0 = 873$ K and a decreasing time width Δt within the range of $1/\nu_F, \ldots, 0$ s, let us "trace" a horizontal line in Fig. 3(a) whose y intercept corresponds to Δt. As Δt decreases (i.e., the line shifts down from 1 s $\rightarrow 0$ s), the long-range relaxations become "frozen" for the smaller subcritical species [e.g., those smaller than a tetramer for $\Delta t=0.5$ s as $t_e(n<4) \geq \Delta t$ at 873 K; see the intercept between the dotted lines in Fig. 3(a)]. This means that the coarsening by atomic exchange of these species is delayed since the growth temperature is abruptly lowered before it happens, which causes the process triggered indeed at an effective temperature $T < 873$ K. In the case shown in Fig. 3(a) (horizontal dotted-dashed line), the chosen time width ($\Delta t = 250$ ms—the optimal one) is short enough [$\Delta t < t_e(n \leq n_c)$ at 873 K] to inhibit the coarsening by atomic exchange (long-range relaxation) of all the subcritical species (those smaller than $n_c=10$ atoms) and is long enough [$\Delta t > t_r(n \leq n_c)$ at 873 K] to allow the short-range relaxations (i.e., the species rearrangements toward 2D shapes by escaping downward) of all of them. This means that the surfaces of films grown with $\Delta t = 250$ ms—FPLD/FPTD [the flattest ones; see Fig. 2(c)]—are mostly populated by a high density of subcritical species that coarsen as slow as possible (at a rate $1/t_i^{pul}$) via atomic incidence while the species keep the morphological relaxation capacity. Shorter T transients ($0 < \Delta t < 250$ ms) reduce the morphological relaxation capacity of the subcritical species [$\Delta t < t_r(n)$ for some $n < n_c$], which produces an effective decrease in n_c and a resulting increase in the roughness. The interpretation of the fully pulsed growth kinetics in terms of balance between short-range and long-range relaxations offers an explanation for the results in Fig. 2(c) that show the Δt dependence of roughness.

A similar analysis to determinate the optimal modulation amplitude ΔT of the T transient was carried out by investigating how the T transient affects the balance between the operative coarsening mechanisms. First of all, let us define the characteristic times of such mechanisms: the times (τ) of formation of n-sized species via the successive aggregation of $n-1$ atoms to monomers were computed as $\tau_x(n) = \sum_{j=1}^{n-1} t_x(j)$ [where $t_x(j) = t_i^{pul}(j)$ and $\tau_x(j) = \tau_i(j)$ or $t_x(j) = t_e(j)$ and $\tau_x(j) = \tau_e(j)$ for species coarsening exclusively via atomic incidence or atomic exchange, respectively] [39]. The dependences of thus-calculated τ_x on the size of the resulting species are shown in Fig. 3(b). On the one hand, $\tau_i(n)$ depends on the flux energy nature [namely, $\tau_i(n) \equiv \tau_i^{th}(n)$ for thermal fluxes without transient mobility—PTD and FPTD—or $\tau_i(n) \equiv \tau_i^{hy}(n)$ for hyperthermal fluxes with transient mobility—PLD and FPLD] and $\tau_i(n)$ is independent of the deposition temperature. The latter means that the use of T transients does modify neither $\tau_i^{th}(n)$ nor $\tau_i^{hy}(n)$. To consider the transient mobility in the calculation of $\tau_i^{hy}(n)$ [$\tau_i^{th}(n)$], $t_i^{pul}(j)$ is replaced with $t_i^{pul}(A_j)$, where $A_j > j$ (or $A_j = j$), as defined in the first term in Eq. (1a), denotes the capture area with [without] transient mobility [19]. On the other hand, $\tau_e(n)$ corresponds to the characteristic time of a series of thermal processes (successive atomic exchanges), and conse-

quently it is affected by T transients. For a given growth temperature and a certain n-sized species, τ_i and τ_e can be taken as the limit formation times, and so any formation process that involves several coarsening mechanisms (e.g., that combines incidences and atomic exchanges) will have a characteristic time within the range of $\min[\tau_e,\tau_i]\ldots\tau_i$. For example [see Fig. 3(b)], the formation time of a septamer ($n=7$) at 873 K by PTD is within the range of $\min[\tau_e,\tau_i^{th}]=\tau_e\approx 3$ s… $\tau_i^{th}=23$ s. This range shrinks to 16–23 s as the temperature decreases down to 813 K and to a single time (when $\tau_e\geq\tau_i^{th}$) of 23 s at 753 K.

The required slow-coarsening condition—defined above as $t_e(n)>t_i^{pul}(n)$–for achieving the lowest roughness implies to delay $\tau_e(n)$ as long as possible so that for all the subcritical species (with $n\leq n_c$) $\tau_e(n)>\tau_i(n)$. As depicted in Fig. 3(b) by means of the vertical arrows, the condition $\tau_e(n)>\tau_i(n)$ is fulfilled (for example) using modulation amplitudes of $\Delta T=120$ K and $\Delta T=60$ K over base temperatures of $T_0=753$ K and $T_0=813$ K [note that for both $T_0+\Delta T=873$ K so that the 2D growth condition $\Delta t>t_r(n)$ at $T_0+\Delta T$ is preserved] for thermal [$\tau_i^{th}(n)<\tau_e(n)$ at T_0] and hyperthermal [$\tau_i^{hy}(n)<\tau_e(n)$ at T_0] pulsed fluxes, respectively. In consequence the species are formed almost exclusively through the atomic incidence on smaller species since the chosen time width $\Delta t=250$ ms of the T transient is $\Delta t\ll\tau_e(n)$ at $T_0+\Delta T$ for any $n>1$. These optimal modulation amplitudes extend the 2D growth regime of the species—referred to right-hand axis in Fig. 3(b)—up to film thickness larger than $F\tau_i^{th}(n_c)=2.6$ ML (for thermal fluxes, FPTD) and $F\tau_i^{hy}(n_c)=0.9$ ML (for hyperthermal ones, FPLD), whereas for growth at constant $T=873$ K (PTD and PLD) the 2D $\rightarrow$3D transition occurs at $F\tau_e(n_c)\geq 0.4$ ML. Modulation amplitudes lower than the optimal ones (e.g., using a T transient with $\Delta T=60$ K and $T_0=813$ K for a growth with thermal pulsed flux) induce a decreases in the surface roughness but without reaching the minimum value since $\tau_i^{th}(n)$ continues being longer than $\tau_e(n)$ at T_0. It means that although the coarsening is slowed, this is still controlled by the atomic exchange at 813 K. On the other hand, modulation amplitudes larger than optimal ones could be experimentally hard to achieve without modifying the time width Δt of the T transient and do not produce a further decrease in the roughness. It is because the species coarsening is controlled by the faster process that in this latter case is the atomic incidence whose characteristic times $t_i^{pul}(n)$ and $\tau_i(n)$ are temperature independent. The fact that the species coarsening caused by the atomic incidence of a thermal pulsed flux is slower than that generated with a hyperthermal pulsed flux—see in Fig. 3(b) how $\tau_i^{th}(n)>\tau_i^{hy}(n)$ for any n—explains why the minimum roughness obtained with FPTD is lower than that resulting from FPLD as shown in Fig. 2(c). This trend is opposed to that found [8,9] in semipulsed growth kinetics, in which the roughness drops as the kinetic energy of the incident species increases from thermal (PTD) to hyperthermal (PLD).

Additionally, the partial freezing of the atomic exchange (and the delay in the species coarsening that this causes) would help us to explain the origin of the high border slopes obtained for FPTD/FPLD-grown structures shown in Fig. 2(b). In absence of atomic exchange, the lateral growth of the structures occurs through short-range morphology relaxations that involve the escape of the incident atoms from atop sites toward the structure borders at the lower terraces. Once the mean species of the kth ML (=kth cross section of the structure) reaches the critical size, the top-layer nucleation of the $(k+1)$th ML prevents the lateral growth giving rise to steep structures. In the case of hyperthermal pulsed fluxes (FPLD), this effect is partially counterbalanced by transient mobility of the incident hyperthermal atoms that acts as a nonequilibrium intralayer transport mechanism enhancing the lateral growth of the structures. This lateral growth starts at the bottom layer of the structures and propagating upward generating structures with lower border slopes.

IV. DISCUSSION

It is worthwhile to compare the method proposed here (the fully pulsed growth kinetics used in FPTD and FPLD) to reduce the surface roughness of PVD-grown films with other similar flattening procedures. The differences between two reported procedures—namely, the well-known "pulsed-laser interval deposition" (PLID) in Ref. [40] and a novel recipe to manipulate the growth kinetics via flux modulation in Ref. [24]—and our method are indicated. Although these reported procedures are valid to reduce the roughness under certain conditions, the simulation reveals that by using our method an additional decrease in the roughness of crystalline surfaces can be expected as discussed below.

PLID [40] consists of a recurrent two-stage growth: a first short interval in which a large amount of material ($\approx$1 unit cell=2 ML) is quickly deposited, followed by a long annealing interval in which no deposition takes place. The PLID method assumes that during the annealing interval, the deposited material recrystallizes, the thickness inhomogeneities are relaxed, and the surface is smoothed. Once the film is recrystallized, the growth continues with a new short deposition—long annealing cycle. However as indicated previously [41], the PLD advantage to generate a high density of surface species that improves the layer-by-layer growth is counterbalanced by the negative effect of multiple deposition on top of small species that occurs when a lot of material is deposited with an intense supersaturated flux. This fact is explained in our model as the 3D growth regime that results from a massive deposition on a shorter time scale than that corresponding to the short-range morphological relaxation $t_i^{pul}(n)<t_r(n)$. In fact, the fast deposition of a $d=2$-ML-thick film without time enough for lateral relaxations (similar to random deposition) produces a rough surface (roughness $\omega=\sqrt{d}$) which is formed by η uncovered MLs, with $\eta>2\sqrt{2}\omega=4$ ML. The rearrangement of this multilayer surface into a flat one (which implies to bypass strong kinetic limitations) requires (i) a long annealing interval (of several dozens of pulse interval $1/\nu_F$), (ii) high annealing temperatures ($\geq 10^3$ K), and (iii) a vicinal substrate that imposes a long-range growth motif. These requirements imply (i) to have tiny deposition rates (or even no deposition for materials with high vapor pressures), (ii) to use thermal stable substrates (e.g., PLID is unsuitable for III-VI semiconductors),

and (iii) to employ substrate surfaces with specific morphologies (indeed, PLID foresees longer annealing intervals for lower surface miscut angles). De facto, the conditions that PLID requires (annealing interval without deposition longer than the lifetime of mobile species on terrace) [42] are only effective to propitiate step-flow growth on vicinal surfaces.

Our method shows a way to overcome the PLID limitations. The strategy to reduce roughness that underlies in the fully pulsed growth kinetics consists of depositing a few of the materials (as few as we are able to rearrange in the interval between pulses) at a high supersaturation with short intense pulses. To increase the deposition rate (in particular on highly corrugated oxide surfaces) up to technologically interesting values [43], the short-range material rearrangement (that involving the morphological relaxations of the surface structures that do not imply coarsening) is speeded up by heating the growing surface over the growth temperature with a time-modulated IR laser. As the simulation demonstrated, yet to confirm experimentally, our method is effective to flat the crystalline surface of films grown with acceptable deposition rates (0.1–1 ML/s) at moderate temperatures on both singular and vicinal substrates since a long-range growth motif is not necessary.

A recent surface x-ray diffraction (SXRD) study [24,44] has revealed that the PLD-type growth kinetics is dominated by nonequilibrium processes that occur during the arrival time of the flux pulse, with a minor contribution of thermal mechanisms. These evidences agree with our simulations [9,16] that demonstrate that the growth kinetics with PLD is ruled by moderate-sized species that (i) coarsen via nonequilibrium mechanisms (such as the atomic insertion and/or the transient mobility of incident hyperthermal atoms) and (ii) are kinetically stable (no species ripening) during the growth time scale. In both works (Refs. [9,44]), the growth proceeds with a three-layer growth front [44] or equivalently with 3 ML height structures [9].

Based on the above evidences [24,44] (SXRD measurements), a promising recipe to manipulate the growth kinetics via flux modulation with the goal of reducing the roughness of PLD-grown films has been postulated [24]. The recipe consists of depositing the material by PLD at a deposition rate (F) that is kept high by increasing the laser repetition rate ν_F progressively whereas the deposition rate per flux pulse (F/ν_F) is decreased accordingly. In short, the recipe intends to change gradually the flux from a pulsed regime (characterized by low ν_F and high F/ν_F) toward a quasicontinuous flux regime (high ν_F and low F/ν_F). In this manner, the high density of nuclei $\rho_{nuclei} \propto F/\nu_F$ generated in the pulsed regime is stabilized against ripening in the quasicontinuous regime and so the initial nuclei density ρ_{nuclei} is preserved. Note that (as shown in Fig. 2 in Ref. [16]) a pulse repetition rate ν_F as high as $\nu_F > 1/t^{n^+} \approx 30$ Hz (where t^{n^+} is defined as the kinetic lifetime of the species) is required to stabilize by PLD species as small as dimers (with $t^{n^+} \approx 33$ ms). Although Christen and Eres [24] do not discard a minor top-layer nucleation after coalescence, they assume that the morphological relaxation of the surface responsible for the ML filling is driven by a nonequilibrium interlayer transport that occurs simultaneously with the incidence and depends only on the growth rate. It means that, in principle, this nonequilibrium transport is independent of the surface feature size to relax.

This latter assumption (namely, a feature-size-independent nonequilibrium transport) is difficult to support because the nonequilibrium mechanisms operate at short range (e.g., the transient mobility is the result of ballistic trajectories of a few lattice parameters [19]) and their effectiveness decays suddenly as the involved lengths increase. Moreover a nonequilibrium transport or relaxation toward lower terraces from inner atop sites of a large island (maybe via insertion of hyperthermal atoms—mechanism *I* in Fig. 1) would be equivalent to consider an atomic implantation phenomenon rather than a process of growth. A plausible explanation could be offered on the basis of considering the formation of fractal-shaped surface structures as a consequence of the early coalescence of close nuclei (as close to each other as $1/\sqrt{\rho_{nuclei}}$). In this case, the nonequilibrium transport depends on the local width of the structure branches, which could change slightly before ML completion, rather than on the structure sizes. The use of a quasicontinuous flux regime as the recipe proposes [24] to induce a ML filling (without ripening) faster than that of "pure" PLD (which is ripening controlled) would reduce quickly the surface fractality by promoting the coalescence of the structure branches. Consequently the above assumption regarding a nonequilibrium transport, which would be independent of the size of the structure to relax, is not longer valid and the morphological relaxation proceeds ruled by thermal processes such as the escape downward (see Sec. III) whose dependence with the feature size is plotted in Fig. 3(a)—compact species size vs relaxation time by escaping downward. Other aspect that Christen and Eres [24] do not take into account is the fact that the species ripening that the proposed recipe tries to avoid is a kinetically limited process [9] under standard PLD conditions and that for example at $\nu_F = 10$ Hz, the ripening is effective only for dimers and trimers as discussed in Ref. [16]. Based on these considerations, it could be expected that the postulated recipe [24] produces a roughness similar to that obtained by PLD, and in any case this roughness would be higher to those generated in films grown by FPVD and FPLD.

Finally, it deserves to be mentioned that the strategy opposed to that proposed here in which flux and temperature are alternately modulated (not in a recurrent manner) corresponds to a widely used nanostructuring [6] procedure [45] based on dewetting phenomena and recrystallization of pseudoamorphous films deposited at low temperatures.

V. CONCLUSIONS

In summary, we have demonstrated that the use of temperature transients enables the decoupling of short-range relaxations (understood as the structural rearrangement of the single species) and the long-range relaxations (i.e., the size rearrangement of the population of surface species via atomic exchange between neighboring species) so that each

can be selectively activated as a morphological design tool. Thus, the proposed fully pulsed growth kinetics (used in FPTD and FPLD) in which the flux and temperature are simultaneously modulated to enable (to inhibit) short-range (long-range) relaxations provides a useful route [46] for flattening crystalline surfaces of thin films. This kinetics extends the crossover between 2D and 3D growth modes up to coverages larger than those obtained with any other growth kinetics by PVD explored so far and/or previously proposed flattening procedure.

ACKNOWLEDGMENTS

This work was supported by Projects No. ESP2006-14282-C02-02 and No. MAT2007-60686 and the *Ramón y Cajal* program (Spanish Science and Innovation Ministry).

[1] L. F. Phillips, Acc. Chem. Res. **37**, 982 (2004); M. Shoji, Int. J. Heat Mass Transfer **47**, 1105 (2004).
[2] M. Kardar, G. Parisi, and Y.-C. Zhang, Phys. Rev. Lett. **56**, 889 (1986); E. Katzav, M. Adda-Bedia, M. B. Amar, and A. Boudaoud, Phys. Rev. E **76**, 051601 (2007).
[3] M. Roy, K. K. Ray, and G. Sundararajan, Oxid. Met. **51**, 251 (1999).
[4] S. M. Lee *et al.*, Phys. Rev. Lett. **82**, 217 (1999); G. Costantini *et al.*, J. Chem. Phys. **112**, 6840 (2000).
[5] J. Teichert, Phys. Rep. **365**, 335 (2002).
[6] Flattening is understood here as the antonym of nanostructuring.
[7] H. Jenniches *et al.*, Appl. Phys. Lett. **69**, 3339 (1996).
[8] B. Shin and M. J. Aziz, Phys. Rev. B **76**, 085431 (2007).
[9] E. Vasco, C. Polop, and J. L. Sacedon, Phys. Rev. Lett. **100**, 016102 (2008).
[10] Intrinsic roughness refers to roughness resulting from the kinetic roughening inherent in the growth techniques rather than roughness due to the set of experimental parameters, the setup used, and/or the abilities of the researchers involved.
[11] PTD corresponds to the technique previously denoted flash evaporation in Ref. [9], which describes a type of deposition using pulsed thermal evaporation.
[12] S. Esch *et al.*, Surf. Sci. **365**, 187 (1996).
[13] J. M. Pomeroy *et al.*, Phys. Rev. B **66**, 235412 (2002).
[14] As discussed in Ref. [9], whereas the breakup of surface species by the bombardment of the surface with energetic particles is a valid strategy [12,13] to reduce the roughness of films grown with moderately supersaturated continuous fluxes (where the species coarsen via adatom aggregation and coalescence), this strategy produces the opposed effect, i.e., an increase in the roughness in films grown with highly supersaturated pulsed fluxes (where the species coarsen via Ostwald ripening). This effect can be explained on the basis of the linear collision-cascade theory in P. Sigmund Phys. Rev. **184**, 383 (1969) that predicts a decrease in the breakup yield as the average atomic coordination (proportional to the curvature radius) of the target species increases. Thus, the bombardment with energetic particles of a surface generated with a pulsed flux gives rise to a preferential breakup of the smaller species, which enhances the Ostwald ripening and consequently the coarsening of the larger species and islands is sped up.
[15] B. Hinnemann, H. Hinrichsen, and D. E. Wolf, Phys. Rev. Lett. **87**, 135701 (2001).
[16] E. Vasco, New J. Phys. **8**, 253 (2006).
[17] Other than the blue/UV laser used for ablating the ceramic target in PLD.
[18] The kinetic energy ranges describing the interaction of incident particles with the matter were estimated using the TRIM code by J. F. Ziegler *et al.*, *The Stopping and Range of Ions in Solids* (Pergamon, New York, 1985) for a 3-ml-thick Y-stabilized ZrO_2 film (Ref. [25]) interacting with atomic Zr and Y in vacuum. Further details are provided as supplementary material in Ref. [9].
[19] E. Vasco and J. L. Sacedon, Phys. Rev. Lett. **98**, 036104 (2007).
[20] E. W. Montroll and G. Weiss, J. Math. Phys. **6**, 167 (1965).
[21] J. M. Stowell, Philos. Mag. **26**, 349 (1972); J. A. Venables, *ibid.* **27**, 697 (1973).
[22] J. Krug, P. Politi, and T. Michely, Phys. Rev. B **61**, 14037 (2000).
[23] The top-layer nucleation probability estimated as the Poissonian probability that two adatoms deposited with a single flux pulse coexist on an island ($M^k \geq 8$) is given by $P_{nuc} = [M^k F/t_F \nu_F t_r(M^k)] \times \int_0^{t_F} \{\exp[-t' M^k \tilde{F}] \int_{t'}^{\infty} \exp[-t''/t_r(M^k)] \partial t''\} \times \partial t'$, where the double integral describes the probability of no escape downward $\{\approx [1/t_r(M^k)] \int_{t'}^{\infty} \exp[-t''/t_r(M^k)] \partial t''\}$ of an adatom that resides on the island during the incidence time t' (ranging between 0 and t_F) of a new atom. For $t_F \nu_F / M^k F = 1.25$ ms (with $M^k = 8$) and the times of escape $t_r(M^k)$ plotted in Fig. 3(a), $P_{nuc} \geq 0.55$. The top-layer nucleation rate is then $P_{nuc} \bar{N} \geq 0.44$ pulse^{-1} (where $\bar{N} = M^k F/\nu_F$ denotes the number of atoms arriving on the island per pulse). The thus-calculated top-layer nucleation rate is similar to that computed using the mean-field rate-equation approach: $D_1(M^k) \times (M^k \rho_1^k)^2 \approx D_1(M^k) \times \bar{N}^2 \approx 0.44$ pulse^{-1}, which validates our rate-equation based model.
[24] H. M. Christen and G. Eres, J. Phys.: Condens. Matter **20**, 264005 (2008).
[25] E. Vasco and C. Zaldo, J. Phys.: Condens. Matter **16**, 8201 (2004).
[26] Ratio of surface temperatures to melting point for YSZ was $T(t)/T_m \approx 0.25-0.30$.
[27] YSZ parameters: density $\rho = 5.9$ mg/mm^3, specific heat $C_p = 0.45$ J/g K, thermal conductivity $\kappa = 2.5$ mW/mm K, and absorption coefficient for IR $\alpha \approx 50$ mm^{-1}.
[28] Δt-width T transients are generated for a laser-energy density per pulse, laser-pulse width, and laser-repetition rate of $J = \varphi(r_{IR}) I_0 r_{IR}^{-2} t_{IR}$, $t_{IR} = 2\Delta t/3$, and $\nu_{IR} = \nu_F = 1$ Hz, respectively, where $I_0 = 100$ W and $\varphi(x) \propto 1/x^2$ is a dimensionless factor that accounts for the dissipation geometry. In particular, $J/\varphi(r_{IR}) = I_0 r_{IR}^{-2} t_{IR} = 0.36$ J/mm^2 to reach $\Delta T \approx 120$ K on the YSZ surface. From an experimental viewpoint, abrupt changes

in the surface temperature (e.g., 120 K in 50 ms) are feasible due to the low thermal inertia of the surface.

[29] L. Xu, G. Henkelman, C. T. Campbell, and H. Jónsson, Phys. Rev. Lett. **95**, 146103 (2005); A. Karim *et al.*, Phys. Rev. B **73**, 165411 (2006).

[30] Thermodynamic parameters used in the simulation: species-size dependent diffusion barrier [29] $E^d(n)=E_1^d[1+\{n-1\}/10]$ (for monomers $E_1^d=2.0$ eV) [31]; coordination dependent binding energy [19] $E^b(n)\approx E_2^b[p(Z)-1]/[p(1)-1]$ [where $p(Z)=2\exp(-\alpha Z^2)$ for $Z\leq 4$ and $p(Z)=4/\alpha^{32}\sqrt{Z}$ otherwise (with $\alpha\approx 0.011$) is the bond-order function; $Z(n)$ is the coordination of the atoms that for species with sizes smaller than the maximum number of bonds per atom is estimated to be $Z(n)\approx n-1$; and $E_2^b=0.60$ eV is the dimer binding energy]; the dissociation energy of the process with rate Γ_n^i is then $E^{diss}(n,i)=E^d(i)+i(n-i)E^b(n)$ so that the barrier to form a kink at the edge of an island on (001) $SrTiO_3$ (assuming a in-plane coordination $Z_{edge}=3$ for the edge atoms) is $E^{diss}=E_1^d+Z_{edge}E^b(Z_{edge})\approx 3.5$ eV, which is within the experimental range (namely, 3.3–3.8 eV) determined by Lippmaa *et al.* (Ref. [32]); the evaporation barrier, $E_1^e=2.5$ eV.

[31] B. Dam and B. Stauble-Pumpin, J. Mater. Sci.: Mater. Electron. **9**, 217 (1998).

[32] M. Lippmaa *et al.*, Appl. Phys. Lett. **76**, 2439 (2000).

[33] A finite coverage $\theta_c=0.9$ ML has to be chosen as ML-completion onset since the full completion becomes an asymptotic condition: $\theta^k(t\to\infty)=1-e^{-\tilde{F}(t)t}\to 1$.

[34] At early growth stages, a roughness ω implies a uncertainty in the deposited thickness $d\pm\delta d$ of $\delta d\approx\pm\frac{1}{2}(2\sqrt{2}\omega-1)$, and then the representative value $\omega=1$ ML corresponds to $\delta d\approx\pm 1$ ML that is the lowest local thickness uncertainty that can be expected since the atom is the indivisible building block for growth.

[35] Since the borders of the small species have a large numbers of imperfections and low-coordinate atoms, the interlayer transport from atop sites of small species is ruled by thermal mechanisms that do not imply the step-edge barrier crossing, such as the atomic insertion next to the edge and the descent across kinks.

[36] $\Phi(n)\approx\sqrt{n-\Delta}/n-\Delta$ for $n>2$ and $\Phi(n)\approx 1$ otherwise (with $\Delta=2$) corresponds to an approximation to describe the average probability by geometric arguments of escaping downward free sites at the species border [i.e., $\Phi(n)\sim$ the fraction of edge-atop sites of an n-sized compact species in a hexagonal lattice where three occupied nearest-neighboring sites define an atop site at the hollow position]. Thus, for example, a trimer defines one atop site with an escape probability of 1 (the three available neighboring sites are at the lower terrace); a tetramer has two atop sites with probabilities of 2/3 each; a pentamer, three atop sites with probabilities 2/3, 2/3, and 1/3 (average probability=5/9); and so on.

[37] A. C. Barato, H. Hinrichsen, and D. E. Wolf, Phys. Rev. E **77**, 041607 (2008).

[38] In terms of occurrence probability of Poissonian processes, the use of an appropriate T transient (with time width Δt) maximizes the difference between the occurrence probabilities ΔP at the incidence time scale $(1/\nu_F)$ of two processes with close rates: one of them (the "activated" process with a characteristic time $\tau'\leq\Delta t$) slightly faster than the other (the "frozen" process with $\tau''>\Delta t$). T transient maximizes ΔP by speeding the faster process up differentially. Thus, it can be demonstrated numerically on the basis of comparing ΔP for the two processes occurring at a constant T:

$$\Delta P[T_{const.}]=\int_0^{1/\nu_F}\{\exp[-t/\tau'(T_{const.})]/\tau'(T_{const.})-\exp[-t/\tau''(T_{const.})]/\tau''(T_{const.})\}\,\partial t$$

with ΔP computed for a square-pulse T—transient with amplitude ΔT over a base temperature T_0 and pulse width Δt

$$\Delta P[T_{trans.}]=\int_0^{\Delta T}\{\exp[-t/\tau'(T_0+\Delta T)]/\tau'(T_0+\Delta T)-\exp[-t/\tau''(T_0+\Delta T)]/\tau''(T_0+\Delta T)\}\,\partial t+\int_{\Delta T}^{1/\nu_F}\{\exp[-t/\tau'(T_0)]/\tau'(T_0)-\exp[-t/\tau''(T_0)]/\tau''(T_0)\}\,\partial t$$

that $\Delta P[T_{const.}]\leq\Delta P[T_{trans.}]$ for any $T_{const.}$ and Δt ranging between $T_0\ldots T_0+\Delta T$ and $\tau'(T_0+\Delta T)\ldots\tau''(T_0+\Delta T)$, respectively.

[39] Note that the mechanism of escaping downward corresponds to a short-range morphological relaxation that does not produce species coarsening.

[40] D. H. A. Blank *et al.*, Appl. Phys. A: Mater. Sci. Process. **69**, 17 (1999).

[41] B. Hinnemann, H. Hinrichsen, and D. E. Wolf, Phys. Rev. E **67**, 011602 (2003).

[42] W. Hong *et al.*, Phys. Rev. Lett. **95**, 095501 (2005).

[43] M. Strikovski and J. H. Miller, Appl. Phys. Lett. **73**, 1733 (1998).

[44] J. Z. Tischler *et al.*, Phys. Rev. Lett. **96**, 226104 (2006).

[45] F. Silly and M. R. Castell, Phys. Rev. Lett. **96**, 086104 (2006).

[46] C. Polop and E. Vasco, Spanish Patent No. P20,0802,388 (8 August 2008).